CHEMISTRY OF MATERIALS

Article

pubs.acs.org/cm

Two-Dimensional Mesoporous Cobalt Sulfide Nanosheets as a Superior Anode for a Li-Ion Battery and a Bifunctional Electrocatalyst for the Li−O_2 System

Palanichamy Sennu,[†] Maria Christy,[‡] Vanchiappan Aravindan,[§] Young-Gi Lee,[∥] Kee Suk Nahm,*[,‡] and Yun-Sung Lee*[,†]

[†]Faculty of Applied Chemical Engineering, Chonnam National University, Gwang-ju 500-757, Republic of Korea

[‡]R&D Education Centre for Fuel Cell Materials & Systems, Chonbuk National University, Jeonju 561-756, Republic of Korea

[§]Energy Research Institute @ NTU (ERI@N), Nanyang Technological University, Research Techno Plaza, 50 Nanyang Drive, Singapore 637553

[∥]Power Control Device Research Team, Electronics and Telecommunications Research Institute, Daejeon 305-700, Korea

Supporting Information

ABSTRACT: We report the synthesis of two-dimensional (2D) Co_3S_4 in a nanothickness sheetlike morphology via simple hydrothermal process and its application to electrochemical energy-storage devices. The presence of unique mesopores with a combination of core/shell nanoparticles in the nanosheets showed superior electrochemical performances as a negative electrode for a Li-ion battery (LIB) and an electrocatalyst in Li−O_2 battery applications. A high discharge capacity of ∼968 mAh g^{-1} is noted after 60 cycles with excellent cycling stability when evaluated as an anode for a LIB. On the other hand, the first discharge capacity of ∼5917 mAh g^{-1} is observed with a high reversibility of 95.72% for the Li−O_2 battery point of view. This exceptional electrochemical performance in both applications is mainly attributed to the presence of mesoporous with core/shell 2D nanostructure, which translates more catalytic bifunctional (oxygen reduction reaction/oxygen evolution reaction) active sites for Li−O_2 and sustains the volume variations that occur in a three-dimensional manner upon the charge−discharge process for LIB applications. *Ex situ* studies, such as transmission electron microscopy, X-ray photoelectron spectroscopy, and impedance spectroscopy studies, are also conducted to validate the reaction mechanisms.

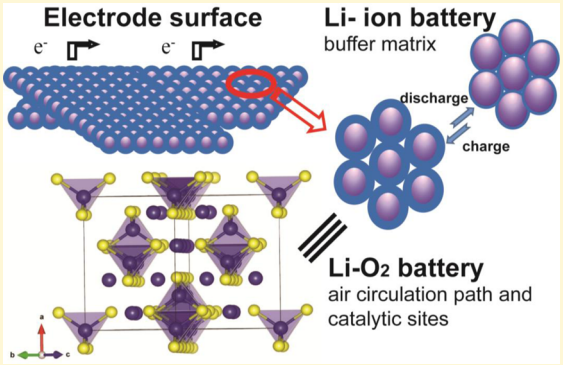

INTRODUCTION

Recently, perovskite-based solar cells and a lithium-air battery (Li−O_2) have been considered as the potential next-generation devices for energy conversion and storage because of their acceptable efficiencies, simple fabrication procedure with low-cost materials, etc.[1−3] A significant improvement in research and development toward energy conversion is noted, for example, Si-based cells, DSSC, and perovskite-based solar cells. On the other hand, apart from a conventional Li-ion battery (LIB), various secondary power systems such as Na ion, Mg ion, Li−S, Li−Se, Li−Te, and Li−O_2 are also explored.[1,2,4] Among them, the Li−O_2 system is found to be appealing in terms of an extremely high energy density (which is comparable to that of gasoline), and oxygen can be obtained from air instead of being provided internally.[4−7] Still, the challenge of complete conversion of its discharge product (Li_2O_2) with minimal overpotential on charge remains. Therefore, catalysts are used for this purpose.[8−10] The performance of the Li−O_2 battery mainly depends on such a catalyst apart from its design (aprotic, aqueous, or solid state).[11] One of the great challenges is to design and synthesize large-surface area bifunctional catalysts on a nanoscale level. In this respect, well-known highly stable catalysts such as Pt, Pd, and RuO_2 are expensive and scarce. Therefore, the noble metal-free catalysts that are composed of earth-abundant elements are important for industrial applications.[6,9] Recently, several low-cost materials, including metal oxides, sulfides, and different carbonaceous materials, are used as catalysts for Li−O_2 battery applications.[12,13] The unique transition metal sulfides (M_xS_y) (x and y = 1, 2, 3, ...) [transition metals (M) were Co, Ni, Mn, Zn, etc.] have been introduced as catalysts for various applications, such as a dye-sensitized solar cell,[14−16] hydro-cracking of vacuum residues, photocatalytic hydrogen evolution, and hydrodesulfurization.[6,17,18] Among them, the cobalt sulfide is worth mentioning as a catalyst and present in various phases such as CoS, CoS_2, Co_3S_4, Co_9S_8, etc., with excellent electrical, magnetic, and

Received: June 15, 2015
Revised: July 25, 2015
Published: August 7, 2015

DOI: 10.1021/acs.chemmater.5b02364
Chem. Mater. 2015, 27, 5726−5735

optical properties.[19] The Co_3S_4 phase exhibits prominent catalytic activity in the aqueous medium oxygen reduction reaction (ORR) and oxygen evolution reaction (OER) compared with those of other reported phases.[19−22] In this vein, we made an attempt to exploit the possibility of using such large-surface area cubic Co_3S_4 as a possible catalyst for Li−O_2 battery applications for the first time.

In addition, Co_3S_4 is also evaluated as an anode for LIB application in half-cell assembly. Because the commercially available graphitic anode endures the problem of Li plating, a lower capacity and a poor high-rate performance are necessary for applications such as hybrid electric vehicles (HEVs) and electric vehicles (EVs).[23−25] Therefore, research activities aimed at developing an alternate anode with high capacity and rate capability have accelerated. Since the discovery of Poizot et al.,[26] for sustained Li storage via conversion reactions other than the conventional intercalation mechanism, numerous metal oxides, sulfides, chlorides, fluorides, etc., have been investigated for negative electrode applications. Generally, cubic phase Co_3S_4 stores the Li via the conversion pathway with a maximal theoretical capacity of ∼702 mAh g^{-1}. However, Co_3S_4 certainly has a few inherent limitations such as large volume changes upon conversion reaction, poor reversibility, and cycle ability. Therefore, very few reports about the battery performance of such an attractive material with respect to the LIB point of view are available.[21] Apart from the fascinating applications of Co_3S_4 in electrochemical energy-storage devices, synthesis of pure cubic phase Co_3S_4 is quite challenging, that too on a nanoscopic level. Hence, for the first time, we report the synthesis of a free mesoporous two-dimensional (2D)-like nanostructure of the Co_3S_4 phase via simple two-step phase transformation from Co_3O_4 nanosheets (Co_3O_4−NS) with a minimal amount of impurities. Eventually, Co_3S_4 nanosheets are studied as negative electrodes for the LIB, and a bifunctional catalyst for the Li−O_2 battery has been systematically evaluated and is described in detail.

EXPERIMENTAL SECTION

Synthesis. The Co_3O_4−NS were used as a sacrificial template for the synthesis of mesoporous Co_3S_4−NS via a facile hydrothermal process.[27−29] In a typical process, 0.2 g of Co_3O_4−NS (see the Supporting Information) was dispersed in 30 mL of deionized water, and 0.3 g of Thioacetamide (Sigma-Aldrich) was also added and the mixture continuously stirred. Then this mixture was transferred into a Teflon-lined stainless-steel autoclave and maintained at 160 °C for 3 h. Subsequently, the reaction temperature was decreased naturally to room temperature, and the products were harvested. The obtained black-brown product was washed with water and ethanol and then dried at 60 °C for 12 h under vacuum. Finally, the black-brown product was calcined at 300 °C (CS-3 NS) and 400 °C (CS-4 NS) in a tube furnace under a N_2 atmosphere.

Characterization. Power X-ray diffraction (XRD) patterns of the Co_3S_4−NS were collected using an X-ray diffractometer (Rint 1000, Rigaku) with Cu Kα radiation. The phase transformation was determined by thermogravimetric analysis (TGA) from ambient temperature to 1000 °C under a N_2 atmosphere by using a thermal analyzer system (STA 1640, Stanton Redcroft Inc.). The Brunauer−Emmett−Teller (BET) specific surface area of the samples was calculated using an ASAP 2010 surface analyzer (Micromeritics). The morphological features of the powders were examined via scanning electron microscopy (SEM) (S-4700 microscope, Hitachi, Tokyo, Japan) and transmission electron microscopy (TEM) (TecnaiF20, Philips). X-ray photoelectron spectroscopy (XPS) was also performed using a Multilab 2000 with monochromated Al Kα radiation ($h\nu$ = 1486.6 eV). Electrochemical impedance spectroscopy (EIS) measurements were taken using an electrochemical analyzer (SP-150, Bio-Logic). Galvanostatic charge−discharge studies were performed using CR2032 coin type cells in a BTS 2004 (JAPAN) battery tester at room temperature.

Preparation of Electrodes. *Li-Ion Battery.* Composite electrodes were formulated with active material (72%) and Ketjen black (14%, KB, EC600JD) and Teflonized acetylene black (TAB-2, 14%) using ethanol. The composites were pressed on a 200 mm^2 area nickel mesh and dried at 160 °C for 4 h in an oven before cell assembly was conducted. The half-cell was fabricated in an argon-filled glovebox with metallic lithium as the counter and reference electrode. Celgard 3401 was used to separate the metallic Li and composite electrode and filled with a 1 M $LiPF_6$ [1:1 (v/v) EC:DMC, Soulbrain Co., Ltd.] electrolyte solution.

Rotating Ring Disk Electrodes (RRDEs) for ORR and OER. For ORR and OER studies, the synthesized Co_3S_4−NS was mixed with carbon powder (Cabot Vulcan XC-72) in 3:7 ratios to ensure sufficient electronic conductivity. Ten milligrams of the mixture described above was dispersed ultrasonically in 150 μL of a diluted Nafion alcohol solution (5 wt %) dissolved in isopropyl alcohol (IPA) to prepare catalyst ink. Approximately 13.5 μL of the catalyst ink (containing 20 μg of catalyst) was loaded onto a glassy carbon electrode and air-dried. The Pt wire and Hg/HgO were used as the counter and reference electrodes, respectively. For the purpose of comparison, Co_3O_4−NS and 30 wt % Pt/C (Premetek Co.) were also studied. Prior to the linear sweep voltammogram (LSV) measurement, O_2 was bubbled directly into the cell for at least 1 h.

Li−O_2 Battery. The synthesized Co_3S_4−NS were used as a catalyst for an air cathode in the Li−O_2 system. The Co_3S_4−NS catalyst and Ketjen black (KB) were mixed in a 1:2 ratio with TAB-2 binder in IPA and made into a pellet type electrode. The pellet was pressed on a Ni mesh current collector, dried overnight at 100 °C, and employed as a cathode. The performance of a Co_3S_4−NS catalyst for ORR and OER in a Li−O_2 air cathode was evaluated in a Swagelok type cell with 1 M LiTFSI in a TEGDME solution and a metallic Li anode. The Li−O_2 cell performance was tested galvanostatically in a potential window of 2−4.3 V vs Li at different current densities (0.1−0.3 mA cm^{-2}) at room temperature with 1 atm of O_2 pressure.

RESULTS AND DISCUSSION

Structural and Morphological Properties. The phase compositions and crystallinity of the prepared samples were examined by powder XRD analysis. In Figure 1a, the presence of observed diffraction peaks is indexed according to the cubic phase of Co_3S_4. The observed reflections are in good agreement with standard XRD patterns (ICSD Card No. 98-002-4212).[28−30] We should note that the peak intensities increased with an increase in post-treatment temperature from 300 to 400 °C. Increasing post-treatment also leads to the formation of inevitable secondary phases such as CoS and Co_9S_8, which is clearly evident from the appearance of reflections at 2θ values of 36°, 48°, and 53°. Thus, like most of the characterizations such as XPS, morphological studies were performed only for CS-4 NS. TGA was also performed under a nitrogen atmosphere to understand the decomposition process and associated phase transition of Co_3S_4 (Figure S1). The observed conversions of CoS_2 (I) to Co_3S_4 (II), CoS (IV), and finally Co_9S_8 (V) at 1000 °C are consistent with the theoretical predictions of weight loss measurement.[31]

The N_2 adsorption−desorption studies were conducted for Co_3S_4−NS prepared under two different conditions and are given in Figure 1b. The N_2 adsorption isotherms of both samples exhibit a type IV H3 hysteresis loop appearing at a high P/P_0 range from 0.8 to 1.0. In the observed isotherms, the hysteresis loop exhibits the saturated adsorption platform that indicates uniform pore formation. CS-3 NS shows a calculated

DOI: 10.1021/acs.chemmater.5b02364
Chem. Mater. 2015, 27, 5726−5735

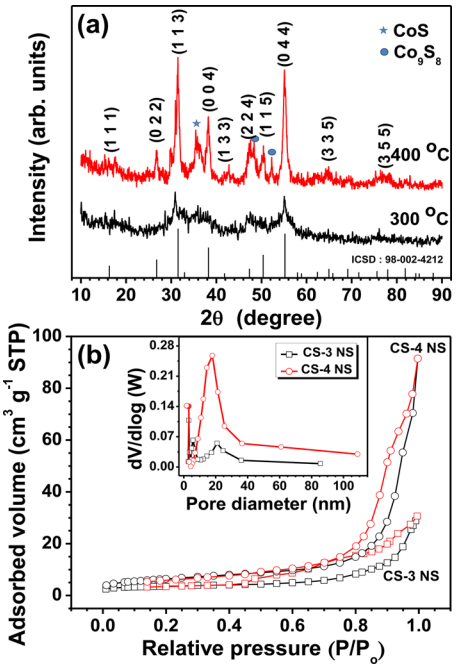

Figure 1. (a) XRD patterns of the pristine Co_3S_4–NS prepared at 300 and 400 °C. (b) N_2 adsorption–desorption isotherms for pristine CS-3 NS and CS-4 NS. The inset shows the characteristic BJH pore size distributions.

BET specific surface area of 12.26 $m^2\ g^{-1}$ and a total pore volume of 0.04738 $cm^3\ g^{-1}$, whereas a BET specific surface area of 23.21 $m^2\ g^{-1}$ and a total pore volume of 0.1413 $cm^3\ g^{-1}$ are noted for CS-4 NS. From the pore size distribution analysis, both CS-3 NS and CS-4 NS exhibit average narrow pore size distributions, mainly around 15–24 nm. Obviously, the specific surface areas of CS-4 NS increases with an increase in temperature from 300 to 400 °C. This is mainly attributed to the removal of organic and sulfur moieties. The large specific surface area possibly provides more active sites in the nanosheets, which could be favorable low-resistance pathways for charge transport upon electrochemical reactions during the charge and discharge process. Also, this feature certainly enhances the electrocatalytic activity irrespective of organic or aqueous media.

The morphological features of Co_3S_4–NS were selectively examined by FE-SEM and HR-TEM studies and are given in Figure 2a–f (Figure S2). A large number of regular rectangular-shaped sheets with dimensions of ~5–8 mm on each side and ~50–80 nm in uniform thickness are evident in Figure 2b. The TEM image confirms the presence of a great number of nanoparticles with the internal carbon-linked structure of the nanosheets, a lateral size much larger than their thickness with conventional mesopores would effectively maintain the long-standing existence of the architectures after phase transformation. The elemental mapping reveals the existence and uniform distribution of cobalt and sulfur elements in the selected nanosheets (Figure 2e). In addition, the crystalline nature of CS-4 NS was realized by HR-TEM and the selected area electron diffraction (SAED) pattern given in Figure 2f. The measured lattice spacings of 0.24 and 0.56 nm correspond to the interlayer spacing of the (004) and (111) crystal planes of Co_3S_4, respectively.[29,32] These also confirm the formation of single-crystal particulates. However, the SAED pattern indicates the presence of polycrystalline-like features, which is mainly caused by the overlap of single-crystalline Co_3S_4 particulates upon TEM analysis.

In addition, detailed information about the chemical composition of the product (CS-4 NS) was validated by XPS measurements and is shown in Figure 3a. The survey spectrum shows the appearance of distinct peaks due to Co 2p, S 2p, C 1s, and O 1s. The Co 2p core level spectra contain two main peaks associated with Co $2p_{3/2}$ and Co $2p_{1/2}$ levels, and the spin–orbit splitting is found to be 15.4 eV, which clearly suggests the formation of Co_3S_4; further deconvolution into four sublevels is shown in Figure 3b. The first doublet peaks at 778.7 and 794.1 eV and second pair at 781.13 and 796.6 eV were assigned to Co^{3+} and Co^{2+} ions, respectively.[19,33] The relative intensity and area of the main $2p_{3/2}$ line indicate the majority of Co^{3+} (approximately 2 for Co^{3+}/Co^{2+}). In addition, the S 2p and C 1s peaks are depicted in Figure S3. The binding energies for S $2p_{3/2}$ and S $2p_{1/2}$ are 161.2 and 162.8 eV, respectively, which correspond to the binding energies of Co–S bonds.[33−35] The peaks at 168.5 and 169.5 eV indicate that an inconsequential amount of C_xSO_y compounds was also formed during the hydrothermal process and surface absorption of oxygen with sulfur. The binding energy of the C 1s main peak at 284.3 eV is due to the graphite-like sp^2 carbon,[30,35] which indicates that the carbon atoms present in a conjugated honeycomb lattice structure. In addition to the main peak, other small peaks are also present at 285.7 and 287.5 eV, which are due to the C–O and C–S bonds arising from the substitution of O and S atoms, respectively. Also, the carbons with sulfur-containing groups have the best donor–acceptor properties with the highest charge mobility in the matrix for enhancing catalytic activity in electron-transfer reactions.

Lithium-Ion Battery. Via preliminary electrochemical studies, CS-4 NS were evaluated as anodes in a half-cell assembly with metallic Li. The half-cell was explored for cyclic voltammetry (CV) studies to understand the Li-storage mechanism, and corresponding traces are given in Figure 3c. In the first cathodic sweep, three reduction peaks were observed at ~1.25, ~0.99, and ~0.64 V vs Li. Similarly, three prominent oxidation peaks appeared at ~1.0, ~1.31, and ~2.04 V vs Li. From the second cycle onward, the reduction peaks were shifted toward higher voltage ranges, for example, shifting from ~1.24 to ~1.7 V vs Li and from ~1.06 to ~1.32 V vs Li, which are noted upon a cathodic sweep. Similarly, a marginal deviation from the peak positions is noted during the anodic scan. However, the area underneath the curves between the first and subsequent cycles is entirely different, which is mainly because of the decomposition of electrolyte solutions in the first discharge along with structural destruction of Co_3S_4. Decomposition of the electrolyte solution certainly leads to the formation of a solid electrolyte interface (SEI), which consumes more Li and results in the huge area under the curve. In the subsequent cycles, only a negligible amount of SEI formation takes place. The overall Li-storage mechanism can be described as follows

$$Co_3S_4 + xLi^+ + xe^- \rightarrow Li_xCo_3S_4$$

$$Li_xCo_3S_4 + (8 - x)Li^+ + (8 - x)e^- \rightarrow 3Co^0 + 4Li_2S$$

$$Co^0 + Li_2S \leftrightarrow Co_9S_8$$

Galvanostatic charge–discharge studies were performed for CS-4 NS at a current density of 0.05A g^{-1} between 0.05 and 3.0 V vs Li and presented in Figure 4a. The Li-storage performance of CS-3 NS was also studied for comparison.

DOI: 10.1021/acs.chemmater.5b02364
Chem. Mater. 2015, 27, 5726–5735

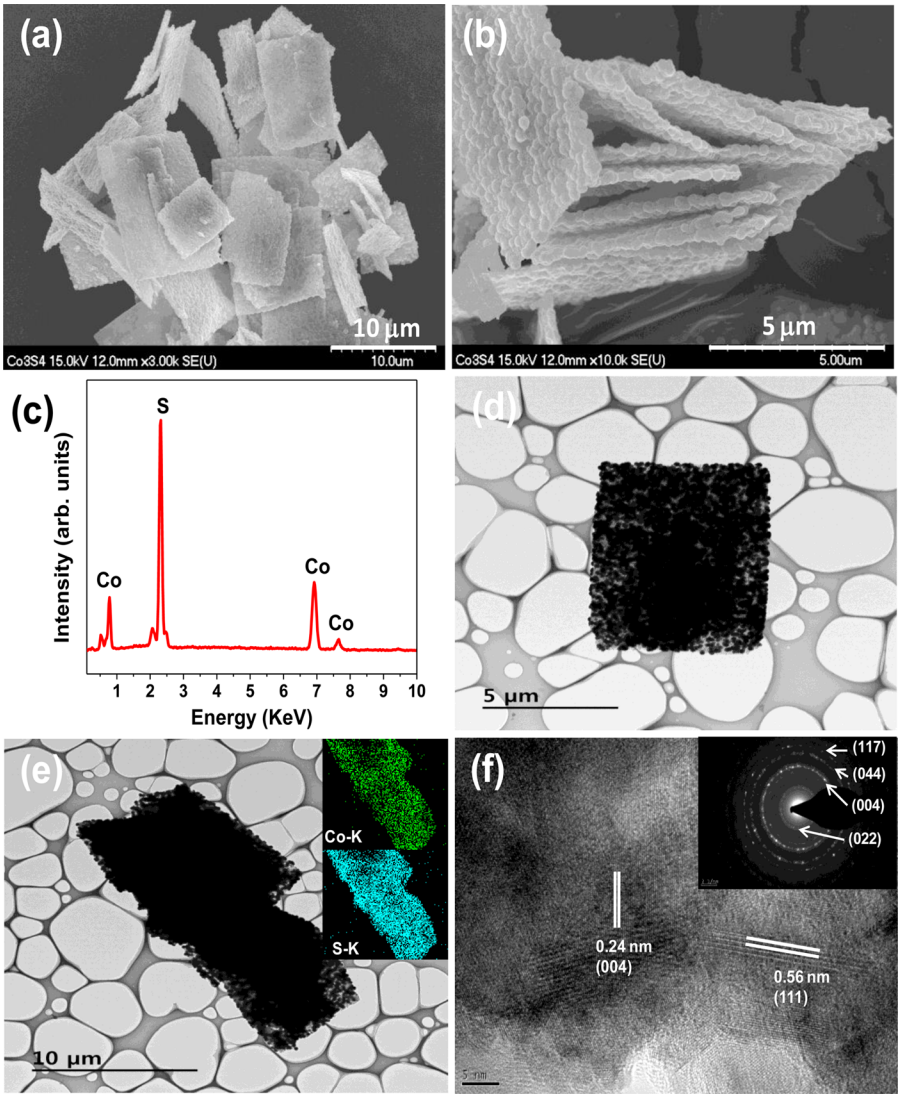

Figure 2. (a) FE-SEM images and EDAX spectrum of pristine CS-4 NS. (b) FE-SEM image showing the sheet thickness. (c) Elemental composition of Co_3S_4-NS. (d) TEM image showing the existence of mesopores. (e) Elemental mapping of CS-4 NS. (f) HR-TEM image and SAED pattern of the CS-4 NS.

We should note that there is no difference between the shape of charge−discharge curves between CS-4 NS and CS-3 NS. Furthermore, the observed slopes and/or plateaus during the charge−discharge process are consistent with the peak positions observed from the CV measurements. The half-cell delivered capacities of ∼1654 and ∼984 mAh g^{-1} for CS-4 NS and ∼1583 and ∼906 mAh g^{-1} for CS-3 NS for the first discharge and charge, respectively. Although less reversible capacity is noted for CS-3 NS, they experience greater irreversible capacity loss (ICL) (∼677 mAh g^{-1}) than CS-4 NS (∼660 mAh g^{-1}). The observed ICL is mainly caused by electrolyte decomposition and subsequent SEI formation in each case. Also, the inevitable side reaction with an electrolyte solution for CS-3 NS cannot be ruled out. Besides, the CS-4 NS exhibit excellent cycling stability and improved Coulombic efficiency compared to those of CS-3 NS for approximately 60 cycles (Figure 4b). The presence of free-standing 2D-like nanosheets with mesoporosity is one of the main reasons for better electrochemical activity, which is certainly beneficial for the permeation of more electrolytes and, thus, provides more active sites for Li storage. Furthermore, the appearance of secondary phases like CoS and Co_9S_8 is also involved in the Li-storage process along with Co_3S_4, which cannot be ignored for the enhanced electrochemical activity of CS-4 NS. However, the capacity fading of CS-3 NS during the course of probably complicated side reactions may result in structural transformations and the irreversibility of sulfur ions. Hence, a reversible capacity of ∼642 mAh g^{-1} (∼71%) was retained after only 60 cycles compared to ∼954 mAh g^{-1} for CS-4 NS (retention of ∼96%). Compared with previous reports on the Co_3S_4/graphene composite, the pristine Co_3S_4−NS delivered excellent battery performance.[17,21,36−38] In addition, it is worth mentioning that the shape of the discharge curves of CS-4 NS remains the same after 60 cycles, whereas dramatic changes in the nature of the curves are noted for CS-3 NS. We strongly believe that it is mainly because of the excellent robustness and highly crystalline nature of the Co_3S_4 nanostructures sintered at 400 °C compared to 300 °C. To confirm the results described above and validate the reaction mechanism, we have conducted *ex situ* studies for the CS-4 NS electrode that will be discussed here.

Figure 5a shows the long-term cyclability of CS-4 NS at two different current densities such as 0.5 and 0.7 A g^{-1} with

DOI: 10.1021/acs.chemmater.5b02364
Chem. Mater. 2015, 27, 5726−5735

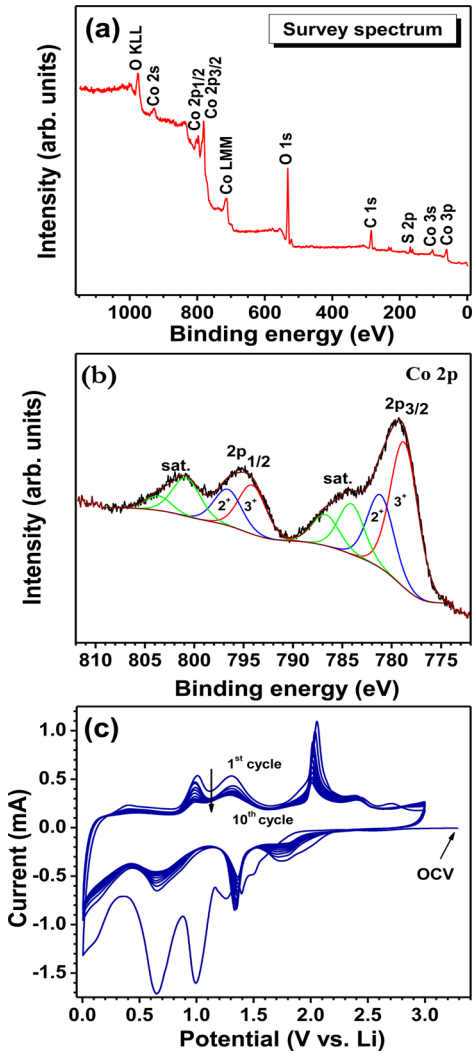

Figure 3. XPS spectra of CS-4 NS: (a) survey and (b) Co 2p. (c) Cyclic voltammogram of CS-4 NS collected at a slow scan rate of 0.1 mV s^{-1} between 0.01 and 3 V vs Li at room temperature.

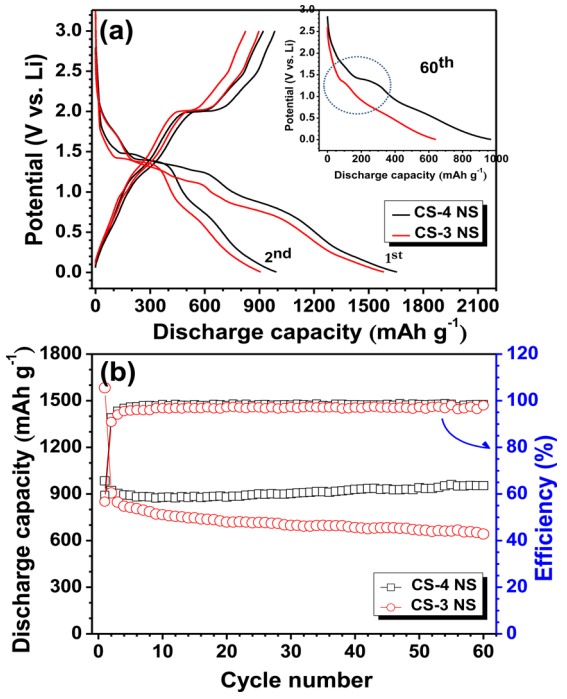

Figure 4. (a) Discharge and charge profile and (b) cycling performance of the pristine CS-3 NS and CS-4 NS vs the Li electrode at a current density of 0.05 A g^{-1} with Coulombic efficiency.

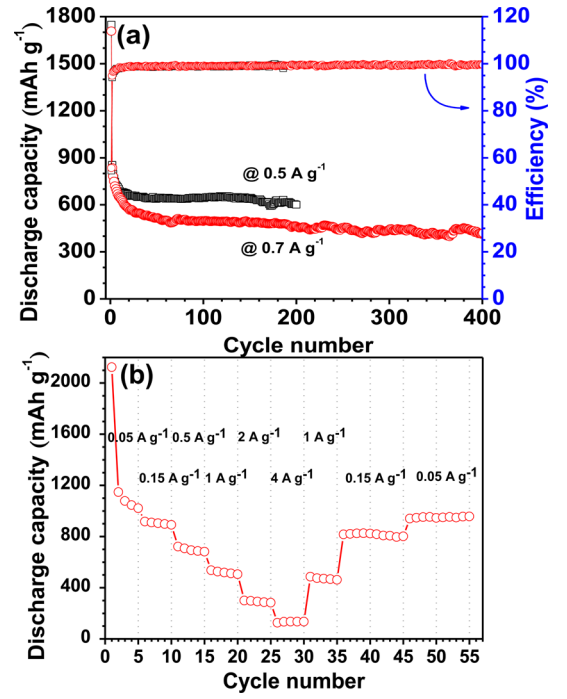

Figure 5. (a) Cycling performance at current rates of 0.5 and 0.7 A g^{-1}. (b) Rate capability of the CS-4 NS vs Li performed at various current rates of 0.05, 0.15, 0.5, 1, 2, and 4A g^{-1}.

Coulombic efficiency. Apart from the anticipated ICL, the cell delivered discharge capacities (second cycle) of ~853 and ~835 mAh g^{-1} at current densities of 0.5 and 0.7 A g^{-1}, respectively. The discharge capacity remains ~600 mAh g^{-1} after 200 cycles at a current density of 0.5 A g^{-1}. On the other hand, a capacity of ~416 mAh g^{-1} is noted after 400 cycles at a current density of 0.7 A g^{-1}. In both cases, the discharge capacity is much higher than the theoretical capacity of a conventional graphitic anode (372 mAh g^{-1}). In addition, it is worth mentioning that, except in the few initial cycles, Coulombic efficiency is found to be >99% irrespective of the current rates. This clearly parallels the Li-storage properties achieved in this work that are superior to those of previous reports.[19,21] Rate capability studies are also conducted for CS-4 NS and shown in Figure 5b. Discharge capacities of ~1024, ~917, ~721, ~536, ~299, and ~126 mAh g^{-1} are observed at current densities of 0.05, 0.15, 0.5, 1, 2, and 4 A g^{-1}, respectively. Remarkably, when the applied current density was switched back after 30 cycles from 4 to 1, 0.15, and 0.05 A g^{-1} imposed on the electrode, the capacity could recover to values of ~486, ~816, and ~940 mAh g^{-1}, respectively. The results revealed the electrode exhibits good structural integrity and is free from particle agglomeration because of the presence of mesopores and carbon between the nanoparticle, which acts as a buffer matrix to uphold the volume variation that occurred upon redox reactions.

Li-ion transport kinetics in LIB was studied using electrochemical impedance spectroscopy (EIS) in the two-electrode coin cell geometry and is presented in Figure 6a. An impedance spectrum was recorded before and after cycling (500 cycles), which is generally composed of three main regions. The depressed

DOI: 10.1021/acs.chemmater.5b02364
Chem. Mater. 2015, 27, 5726−5735

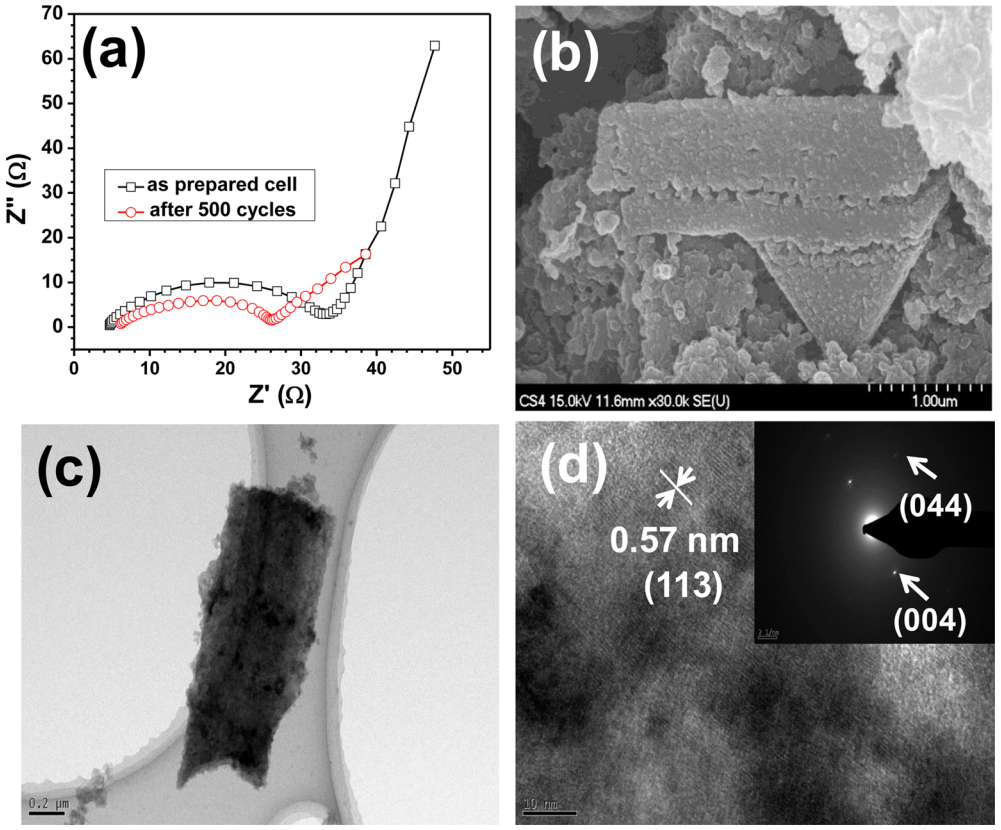

Figure 6. (a) Comparison of Nyquist plots before and after 500 cycles for the CS-4 NS electrode. (b) FE-SEM picture of the CS-4 NS electrode after 500 cycles. (c) TEM image of the CS-4 NS electrode after 500 cycles. (d) High-resolution TEM image and SAED pattern of the CS-4 NS electrode recorded after 500 cycles.

semicircles in the high-frequency region are associated with the electrolyte resistance (Rs), and the high- to middle-frequency region is assigned to the contact and charge-transfer resistance across the electrode/electrolyte interface (Rct). Finally, the vertical tail inclined at the 45° low-frequency region, as one would expect for capacitance behavior (Warburg element). The Rs and Rct values are found to be 5.38 and 34.5 Ω, respectively, before cycling. After cycling, the Rct values are decreased dramatically from 34.5 to 26.72 Ω, which may be related to the stabilization of the SEI layer. The mesopores and core−shell carbon in a sheet structure can accommodate more electrolytes, which may facilitate interfacial charge transfer at the electrode/electrolyte interface on a nanoscale level. The level of electrolyte wetting through mesopores is gradually increased and eventually translates to a beneficial effect on the stabilization of the SEI layer. Furthermore, to substantiate the structural integrity of anodes after cycling, the half-cell was carefully dismantled (in a charged state, i.e., 3 V vs Li) and examined via SEM and TEM. The CS-4NS electrode retained same sheetlike morphology after 500 prolonged galvanostatic cycles (Figure 6b,c and Figure S3c,d). This confirms the robustness and structural integrity of the Co_3S_4 prepared at 400 °C. Further, the SAED pattern,[15,39,40] cobalt and sulfur results from the XPS spectrum, recorded in the charged state clearly confirms the formation of Co_9S_8 rather than Co_3S_4 during the charge process. Overall, we strongly believe that the presence of mesoporosity with a two-dimensional sheetlike morphology is responsible for the excellent high rate, high capacity, and stability of this fascinating conversion type anode. Even further, this mesoporous Co_3S_4 nanosheet exhibits electrochemical performance better than that of nanotube and nanosheet morphology reported elsewhere by others.[19,21] Although ICL is observed for such Co_3S_4 nanosheets, it is certainly overcome by the prelithiation process during the construction of a full cell assembly with conventional cathodes. Therefore, Co_3S_4 could be used as a promising contender high-power anode in LIB applications.

Electrocatalytic Properties. To study the catalytic activity of synthesized Co_3S_4 phases at different calcination temperatures, only CS-4 NS has been subjected to investigation. A well-known catalyst, Pt/C, was also evaluated under the same testing condition for comparison. The catalytic activity of CS-4 NS is qualitatively estimated from the oxygen reduction reaction, and the reduction peak potentials measured in CV traces are illustrated in Figure 7a. The CV curves of CS-4 NS and sacrificial Co_3O_4 NS with respect to Pt/C electrodes in a 0.1 M KOH solution show saturation with O_2 at a sweep rate of 5 mV s^{-1}. All the electrodes exhibited a well-defined cathodic peak, while the CS-4 NS (−0.205 V) peak position is more positive than that of Co_3O_4 NS (−0.221 V) and comparable to that of Pt/C (−0.095 V).[41] A catalyst with higher electrochemical activity toward the ORR will demonstrate a positively shifted reduction peak potential. Hence, we compared it with a Pt/C electrode to investigate the electron transfers upon the ORR response with our catalyst, CS-4 NS. Though CS-4 NS exhibits higher negative potential (~110 mV), it is still comparable and less expensive than the Pt/C catalyst. In addition, CS-4 NS displayed a current drop with a positively shifted onset potential and a steady state current higher than that of Co_3O_4 NS. Therefore, this significant response of our new catalyst, CS-4

DOI: 10.1021/acs.chemmater.5b02364
Chem. Mater. 2015, 27, 5726−5735

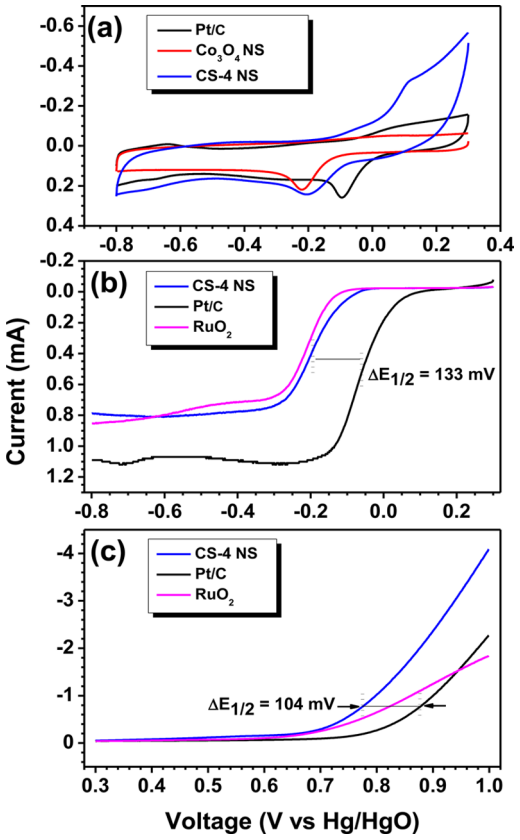

Figure 7. Characteristic comparison of (a) cyclic voltammograms, (b) ORR, and (c) OER of the pristine CS-4 NS (blue line) with commercial Pt/C (black line) and RuO_2 (pink line) as catalysts in an O_2-saturated 0.1 M KOH solution at a scan rate of 5 mV s^{-1}.

NS, will certainly be useful for metal air battery applications, preferably the Li−O_2 system.

To employ CS-4 NS as an efficient catalyst for Li−O_2 systems, ORR and OER activities were studied using LSV. This LSV has been recorded via RRDE with a rotation speed of 1600 rpm in O_2-saturated 0.1 M KOH as an electrolyte solution at a scan rate of 5 mV s^{-1}. Figure 7b represents the comparative ORR activities of CS-4 NS with commercial RuO_2 and Pt/C recorded between 0.3 and −0.8 V vs Hg/HgO. The onset potential of CS-4 NS (−0.066 V) is slightly lower than that of Pt/C (0.05 V) but still comparable to that of Pt/C, which makes it a good ORR catalyst. Further, OER properties from LSV polarization curves were recorded during an anodic scan (5 mV s^{-1}) between 0.3 and 1.0 V vs Hg/HgO (Figure 7c) compared to commercial RuO_2. It is clearly observed that using the onset potential, CS-4 NS (0.559 V) is a better OER catalyst than the commercial RuO_2 (0.59 V). This explains the bifunctional electrocatalytic property of the synthesized Co_3S_4 material.[19−21,42,43] To improve our understanding, quantitative bifunctional activities of CS-4 NS are listed in Table 1. The cobalt can exchange sulfur atoms with the electrolyte and relevant changes in oxidation states from +2 to +3 to +4 at near-equilibrium potentials, which could potentially facilitate ORR and OER chemistry. Further, the intrinsic tunnels of the cubic phase Co_3S_4 crystalline lattice and its mesoporous core/shell carbon also act as bifunctional activity in aqueous electrolytes. This result clearly suggests the superior electrocatalytic properties of CS-4 NS are suitable for a precise air cathode catalyst in a Li−O_2 battery. Because it is not easy to analyze the ORR and OER performance in nonaqueous electrolytes, we directly applied our synthesized catalyst (CS-4 NS) as a cathode material in a Li−air battery and systematically examined the electrocatalytic properties.

Li−O_2 Battery. The electrochemical performance of the CS-4 NS catalyst in the air cathode was evaluated in Swagelok type Li−O_2 cells. The electrochemical reaction of the Li−O_2 cell can be expressed as $2(Li^+ + e^-) + O_2 \rightleftarrows Li_2O_2$, during which ORR and OER take place upon the discharge (forward) and charge (reverse) process, respectively.[6,10,44,45] The charge−discharge studies for Li−O_2 cells were conducted between 2 and 4.3 V vs Li at a current density of 0.1 mA cm^{-2} (0.1 A g^{-1}), in which CS-4 NS-catalyzed KB was used as an air cathode (Figure 8a). Pure KB was also used (without CS-4 NS) as an air cathode under the same conditions for comparison. The first discharge capacity of CS-4 NS is found to be ∼5917 mAh g^{-1} with a very flat discharge plateau at 2.7 V vs Li. This obtained discharge capacity is almost twice that of the only KB air cathode (∼3143 mAh g^{-1}). It is obvious that addition of CS-4 NS certainly improved the ORR performance in the air battery. Upon charging, a 95.72% discharge capacity is retained (∼5664 mAh g^{-1}) for the CS-4 NS-catalyzed air cathode, which clearly shows excellent reversibility. The ORR and OER performance in a nonaqueous electrolyte is also consistent with the catalyst performance in aqueous media, which further confirms the excellent bifunctional activity of CS-4 NS. The overpotential (ΔV) is reduced to ∼0.921 V for the CS-4 NS catalyst, which is low and quite favorable for the reversibility of the Li−O_2 battery. The reversibility of the synthesized CS-4 NS electrocatalyst was also tested at different current densities and is given in Figure 8b. It is interesting to note that the maximal discharge capacity of ∼6990 mAh g^{-1} is noted at a current density of 0.2 mA cm^{-2} (0.2 A g^{-1}). In addition, at this current density, maximal reversibility is noted, i.e., ∼99.11% retention upon charging. The battery performance at a current density of 0.2 mA cm^{-2} is much better than the lower current density (0.1 mA cm^{-2}) in terms of capacity and overpotential. At a higher current density of 0.3 mA cm^{-2} (0.3 A g^{-1}), the cell delivered a discharge capacity of ∼5346 mAh g^{-1} with 84.71% retention; however, the observed capacity and reversibility are far better than those of the KB air cathode. Generally, at a low current density, the Li−O_2 system delivers a higher discharge capacity. In contrast, comparatively, a higher capacity with a

Table 1. Comparative CV, ORR, and OER Data for As-Prepared CS-4 NS with Commercial Pt/C and RuO_2 as Catalysts

	CV		ORR		OER		
sample	peak potential (V)	peak current (mA)	onset potential (V)	half-wave potential (V)	onset potential (V)	half-wave potential (V)	limiting current (mA)
Pt/C	−0.095	0.2588	0.05	−0.061	0.681	0.883	−2.27
RuO_2	–	–	−0.11	−0.203	0.593	0.828	−1.84
CS-4 NS	−0.205	0.2428	−0.066	−0.194	0.559	0.7795	−4.087
Co_3O_4 NS	−0.221	0.219	–	–	–	–	–

DOI: 10.1021/acs.chemmater.5b02364
Chem. Mater. 2015, 27, 5726−5735

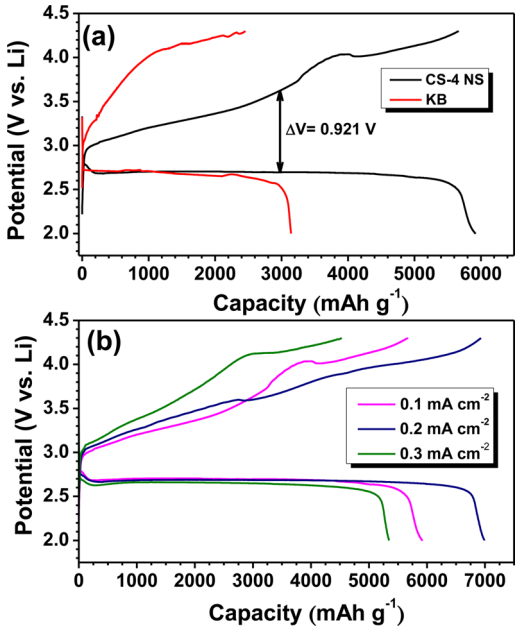

Figure 8. (a) First charge−discharge profile of the Li−O_2 cell with CS-4 NS as the catalyst and pure Ketjen black (KB) at a current density of 0.1 mA cm^{-2} (or 0.1 A g^{-1}). (b) Rate performance of the Li−O_2 cell with the CS-4 NS catalyst with different current densities.

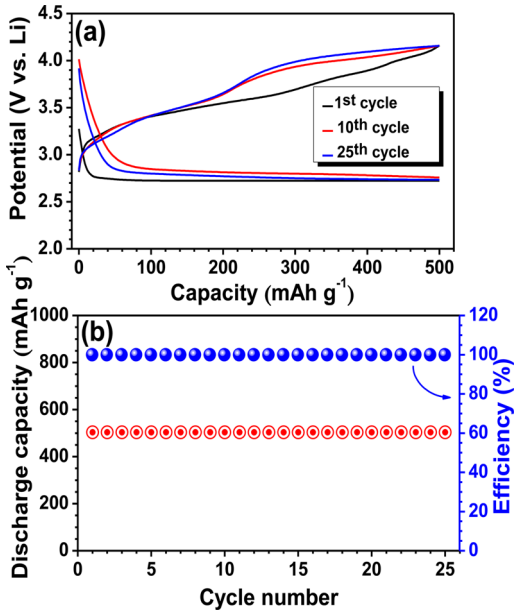

Figure 9. (a) Capacity-limited cycling performance. (b) Capacity vs cycle number of the Li−O_2 cell with a CS-4 NS-catalyzed electrode at a current rate of 0.1 mA cm^{-2} (or 0.1 A g^{-1}).

low overpotential is obtained for a higher current density (0.2 and 0.3 mA cm^{-2}). However, we also previously observed a similar kind of results while employing α-MnO_2 and N-GNF as catalysts for the Li−O_2 system.[45] This finding clearly suggests the CS-4 NS is a promising catalyst to be used in the Li−O_2 system.

To achieve complete stable cycling without any decrease in capacity, we also investigated the cells with a limited depth of discharge.[46,47] Accordingly, the capacity of Li−O_2 cells was limited to 500 mAh g^{-1} at a current density of 0.1 mA cm^{-2} (or 0.1 A g^{-1}), and the corresponding cyclability is given in Figure 9. Stable cycling profiles with no capacity degradation or changes in the nature of the discharge−charge curves for 25 cycles with 100% efficiency can be observed. Figure 9b shows the cycling performance of the Li−O_2 cell with a CS-4 NS-catalyzed electrode at 0.1 mA g^{-1}. From all the observed results, it is inferred that synthesized Co_3S_4 nanosheets calcined at 400 °C can be used as an efficient bifunctional catalyst in both aqueous and nonaqueous media, especially to improve the battery performance in the Li−O_2 cell.

The better electrochemical performances of ordered mesoporous materials as a cathode catalyst for rechargeable Li−O_2 batteries have been well-established.[48] It can be inferred from the BET surface analysis that the synthesized CS-4 NS structure possesses a highly mesoporous surface with a significantly large pore volume compared to that of CS-3 NS. The two-dimensional surface with mesopores helps in the formation and accommodation of Li_2O_2 and thus in turn promotes the decomposition or OER as well in the active sites of the air cathode.[49] This might be the main reason for the superior performance of the air cathode.[50,51] In addition, the CS-4 NS structure seems to be highly conductive and stable, which leads to rapid ion mobility. Apart from the characteristics of the catalyst, the electrolyte also plays an important part in the performance of the battery. In this case, the TEGDME electrolyte has been utilized, which is considered to be one of the best so far and favors better battery performance, as well. Thus, the CS-4 NS electrocatalyst actively promotes the ORR and OER in the Li−air battery and appears to be a suitable air cathode catalyst.

CONCLUSION

Unique mesoporous architecture takes full advantage of volume changes and air diffusion pathways in Li−ion and Li−O_2 systems, respectively. Also, the design of two-dimensional sheetlike core/shell nanostructures presented here ensures superior cycling performance and rate capability in both systems. The pristine Co_3S_4 NS (CS-4 NS) was evaluated as a conversion type anode and maintains a capacity of 600 mAh g^{-1} after 200 extremely stable cycles at a current density of 0.5 A g^{-1}. Interestingly, the phase transition from Co_3S_4 to Co_9S_8 upon electrochemical cycling has been clearly validated by the *ex situ* studies. More inspiringly, the bifunctional electrocatalytic activity was clearly seen in aqueous media and comparable with those of the established catalysts like Pt/C and RuO_2. As a result, with a bifunctional catalyst in the Li−O_2 system, the cell delivered a capacity as high as 6990 mAh g^{-1} at a current density of 0.2 mA cm^{-2}. In addition, excellent stability for capacity-limited cycling with a low potential gap and rate performance were added advantages for this unique material, Co_3S_4 NS. To the best our knowledge, this is the first time mesoporous two-dimensional cobalt sulfides have been introduced as a bifunctional electrocatalyst into Li−O_2 systems, which further opens new avenues for the development of this novel material and its suitability for electrochemical energy-storage applications.

ASSOCIATED CONTENT

Supporting Information

The Supporting Information is available free of charge on the ACS Publications website at DOI: 10.1021/acs.chemmater.5b02364.

Synthesis of Co_3O_4 nanosheets, SEM and XPS of Co_3O_4 and Co_3S_4 nanosheets prepared at different calcination temperatures, and TGA and CV studies (PDF)

DOI: 10.1021/acs.chemmater.5b02364
Chem. Mater. 2015, 27, 5726−5735

AUTHOR INFORMATION

Corresponding Authors

*E-mail: leeys@chonnam.ac.kr.
*E-mail: nahmks@jbnu.ac.kr.

Notes

The authors declare no competing financial interest.

ACKNOWLEDGMENTS

We acknowledge financial support from the R&D Convergence Program of NST (National Research Council of Science & Technology) of the Republic of Korea.

REFERENCES

(1) Bruce, P. G.; Freunberger, S. A.; Hardwick, L. J.; Tarascon, J.-M. Li-O_2 and Li-S batteries with high energy storage. *Nat. Mater.* **2011**, *11*, 19.

(2) Choi, N.-S.; Chen, Z.; Freunberger, S. A.; Ji, X.; Sun, Y.-K.; Amine, K.; Yushin, G.; Nazar, L. F.; Cho, J.; Bruce, P. G. Challenges Facing Lithium Batteries and Electrical Double-Layer Capacitors. *Angew. Chem., Int. Ed.* **2012**, *51*, 9994.

(3) Yu, M.; Ren, X.; Ma, L.; Wu, Y. Integrating a redox-coupled dye-sensitized photoelectrode into a lithium−oxygen battery for photo-assisted charging. *Nat. Commun.* **2014**, *5*, 5111.

(4) Lee, J.-S.; Tai Kim, S.; Cao, R.; Choi, N.-S.; Liu, M.; Lee, K. T.; Cho, J. Metal−Air Batteries with High Energy Density: Li−Air vs Zn−Air. *Adv. Energy Mater.* **2011**, *1*, 34.

(5) Laoire, C.; Mukerjee, S.; Plichta, E. J.; Hendrickson, M. A.; Abraham, K. M. Rechargeable Lithium/TEGDME-$LiPF_6$/O_2 Battery. *J. Electrochem. Soc.* **2011**, *158*, A302.

(6) Abraham, K. M.; Jiang, Z. A Polymer Electrolyte-Based Rechargeable Lithium/Oxygen Battery. *J. Electrochem. Soc.* **1996**, *143*, 1.

(7) Girishkumar, G.; McCloskey, B.; Luntz, A. C.; Swanson, S.; Wilcke, W. Lithium−Air Battery: Promise and Challenges. *J. Phys. Chem. Lett.* **2010**, *1*, 2193.

(8) Trahey, L.; Johnson, C. S.; Vaughey, J. T.; Kang, S.-H.; Hardwick, L. J.; Freunberger, S. A.; Bruce, P. G.; Thackeray, M. M. Activated Lithium-Metal-Oxides as Catalytic Electrodes for Li−O_2 Cells. *Electrochem. Solid-State Lett.* **2011**, *14*, A64.

(9) Débart, A.; Paterson, A. J.; Bao, J.; Bruce, P. G. α-MnO_2 Nanowires: A Catalyst for the O_2 Electrode in Rechargeable Lithium Batteries. *Angew. Chem., Int. Ed.* **2008**, *47*, 4521.

(10) Sun, B.; Munroe, P.; Wang, G. Ruthenium nanocrystals as cathode catalysts for lithium-oxygen batteries with a superior performance. *Sci. Rep.* **2013**, *3*, 2247.

(11) Lu, J.; Li, L.; Park, J.-B.; Sun, Y.-K.; Wu, F.; Amine, K. Aprotic and Aqueous Li−O_2 Batteries. *Chem. Rev.* **2014**, *114*, 5611.

(12) Song, K.; Agyeman, D. A.; Jung, J.; Jo, M. R.; Yang, J.; Kang, Y.-M. A Review of the Design Strategies for Tailored Cathode Catalyst Materials in Rechargeable Li-O_2 Batteries. *Isr. J. Chem.* **2015**, *55*, 458.

(13) Christensen, J.; Albertus, P.; Sanchez-Carrera, R. S.; Lohmann, T.; Kozinsky, B.; Liedtke, R.; Ahmed, J.; Kojic, A. A Critical Review of Li/Air Batteries. *J. Electrochem. Soc.* **2012**, *159*, R1.

(14) Zheng, X.; Guo, J.; Shi, Y.; Xiong, F.; Zhang, W.-H.; Ma, T.; Li, C. Low-cost and high-performance $CoMoS_4$ and $NiMoS_4$ counter electrodes for dye-sensitized solar cells. *Chem. Commun.* **2013**, *49*, 9645.

(15) Chang, S.-H.; Lu, M.-D.; Tung, Y.-L.; Tuan, H.-Y. Gram-Scale Synthesis of Catalytic Co_9S_8 Nanocrystal Ink as a Cathode Material for Spray-Deposited, Large-Area Dye-Sensitized Solar Cells. *ACS Nano* **2013**, *7*, 9443.

(16) Park, J. T.; Lee, C. S.; Kim, J. H. High performance electrocatalyst consisting of CoS nanoparticles on an organized mesoporous SnO_2 film: its use as a counter electrode for Pt-free, dye-sensitized solar cells. *Nanoscale* **2015**, *7*, 670.

(17) Kong, S.; Jin, Z.; Liu, H.; Wang, Y. Morphological Effect of Graphene Nanosheets on Ultrathin CoS Nanosheets and Their Applications for High-Performance Li-Ion Batteries and Photocatalysis. *J. Phys. Chem. C* **2014**, *118*, 25355.

(18) Peng, S.; Li, L.; Tan, H.; Cai, R.; Shi, W.; Li, C.; Mhaisalkar, S. G.; Srinivasan, M.; Ramakrishna, S.; Yan, Q. MS_2 (M = Co and Ni) Hollow Spheres with Tunable Interiors for High-Performance Supercapacitors and Photovoltaics. *Adv. Funct. Mater.* **2014**, *24*, 2155.

(19) Liu, Q.; Zhang, J. A general and controllable synthesis of Co_mS_n (Co_9S_8, Co_3S_4, and $Co_{1-x}S$) hierarchical microspheres with homogeneous phases. *CrystEngComm* **2013**, *15*, 5087.

(20) Wang, H.; Li, Z.; Li, G.; Peng, F.; Yu, H. Co_3S_4/NCNTs: A catalyst for oxygen evolution reaction. *Catal. Today* **2015**, *245*, 74.

(21) Mahmood, N.; Zhang, C.; Jiang, J.; Liu, F.; Hou, Y. Multifunctional Co_3S_4/Graphene Composites for Lithium Ion Batteries and Oxygen Reduction Reaction. *Chem. - Eur. J.* **2013**, *19*, 5183.

(22) Black, R.; Adams, B.; Nazar, L. F. Non-Aqueous and Hybrid Li-O_2 Batteries. *Adv. Energy Mater.* **2012**, *2*, 801.

(23) Aravindan, V.; Lee, Y.-S.; Yazami, R.; Madhavi, S. TiO_2 polymorphs in 'rocking-chair' Li-ion batteries. *Mater. Today* **2015**, *18*, 345.

(24) Aravindan, V.; Sundaramurthy, J.; Suresh Kumar, P.; Lee, Y.-S.; Ramakrishna, S.; Madhavi, S. Electrospun nanofibers: A prospective electro-active material for constructing high performance Li-ion batteries. *Chem. Commun.* **2015**, *51*, 2225.

(25) Aravindan, V.; Lee, Y. S.; Madhavi, S. Research Progress on Negative Electrodes for Practical Li-Ion Batteries: Beyond Carbonaceous Anodes. *Adv. Energy Mater.* **2015**, *5*, 1402225.

(26) Poizot, P.; Laruelle, S.; Grugeon, S.; Dupont, L.; Tarascon, J. M. Nano-sized transition-metal oxides as negative-electrode materials for lithium-ion batteries. *Nature* **2000**, *407*, 496.

(27) Sennu, P.; Kim, H. S.; An, J. Y.; Aravindan, V.; Lee, Y. S. Synthesis of 2D/2D Structured Mesoporous Co_3O_4 Nanosheet/N-Doped Reduced Graphene Oxide Composites as a Highly Stable Negative Electrode for Lithium Battery Applications. *Chem. - Asian J.* **2015**, *10*, 1776.

(28) Chen, Q.; Li, H.; Cai, C.; Yang, S.; Huang, K.; Wei, X.; Zhong, J. In situ shape and phase transformation synthesis of Co_3S_4 nanosheet arrays for high-performance electrochemical supercapacitors. *RSC Adv.* **2013**, *3*, 22922.

(29) Zhao, W.; Zhang, C.; Geng, F.; Zhuo, S.; Zhang, B. Nanoporous Hollow Transition Metal Chalcogenide Nanosheets Synthesized via the Anion-Exchange Reaction of Metal Hydroxides with Chalcogenide Ions. *ACS Nano* **2014**, *8*, 10909.

(30) Wang, Q.; Jiao, L.; Du, H.; Si, Y.; Wang, Y.; Yuan, H. Co_3S_4 hollow nanospheres grown on graphene as advanced electrode materials for supercapacitors. *J. Mater. Chem.* **2012**, *22*, 21387.

(31) Kumar, N.; Raman, N.; Sundaresan, A. Synthesis and Properties of Cobalt Sulfide Phases: CoS_2 and Co_9S_8. *Z. Anorg. Allg. Chem.* **2014**, *640*, 1069.

(32) Yin, Y.; Rioux, R. M.; Erdonmez, C. K.; Hughes, S.; Somorjai, G. A.; Alivisatos, A. P. Formation of Hollow Nanocrystals Through the Nanoscale Kirkendall Effect. *Science* **2004**, *304*, 711.

(33) Grace, A. N.; Ramachandran, R.; Vinoba, M.; Choi, S. Y.; Chu, D. H.; Yoon, Y.; Nam, S. C.; Jeong, S. K. Facile Synthesis and Electrochemical Properties of Co_3S_4-Nitrogen-Doped Graphene Nanocomposites for Supercapacitor Applications. *Electroanalysis* **2014**, *26*, 199.

(34) Ghahremaninezhad, A.; Dixon, D. G.; Asselin, E. Electrochemical and XPS analysis of chalcopyrite ($CuFeS_2$) dissolution in sulfuric acid solution. *Electrochim. Acta* **2013**, *87*, 97.

(35) Wang, G.; Zhang, J.; Kuang, S.; Liu, S.; Zhuo, S. The production of cobalt sulfide/graphene composite for use as a low-cost counter-electrode material in dye-sensitized solar cells. *J. Power Sources* **2014**, *269*, 473.

(36) Liu, S.; Wang, J.; Wang, J.; Zhang, F.; Liang, F.; Wang, L. Controlled construction of hierarchical $Co_{1-x}S$ structures as high performance anode materials for lithium ion batteries. *CrystEngComm* **2014**, *16*, 814.

DOI: 10.1021/acs.chemmater.5b02364
Chem. Mater. 2015, 27, 5726−5735

(37) Wang, Y.; Wu, J.; Tang, Y.; Lü, X.; Yang, C.; Qin, M.; Huang, F.; Li, X.; Zhang, X. Phase-Controlled Synthesis of Cobalt Sulfides for Lithium Ion Batteries. *ACS Appl. Mater. Interfaces* **2012**, *4*, 4246.
(38) Su, Q.; Xie, J.; Zhang, J.; Zhong, Y.; Du, G.; Xu, B. In Situ Transmission Electron Microscopy Observation of Electrochemical Behavior of CoS_2 in Lithium-Ion Battery. *ACS Appl. Mater. Interfaces* **2014**, *6*, 3016.
(39) Zhou, Y.; Yan, D.; Xu, H.; Feng, J.; Jiang, X.; Yue, J.; Yang, J.; Qian, Y. Hollow nanospheres of mesoporous Co_9S_8 as a high-capacity and long-life anode for advanced lithium ion batteries. *Nano Energy* **2015**, *12*, 528.
(40) Luo, F.; Li, J.; Yuan, H.; Xiao, D. Rapid synthesis of three-dimensional flower-like cobalt sulfide hierarchitectures by microwave assisted heating method for high-performance supercapacitors. *Electrochim. Acta* **2014**, *123*, 183.
(41) Liu, Q.; Jin, J.; Zhang, J. $NiCo_2S_4$@graphene as a Bifunctional Electrocatalyst for Oxygen Reduction and Evolution Reactions. *ACS Appl. Mater. Interfaces* **2013**, *5*, 5002.
(42) Feng, Y.; He, T.; Alonso-Vante, N. In situ Free-Surfactant Synthesis and ORR- Electrochemistry of Carbon-Supported Co_3S_4 and $CoSe_2$ Nanoparticles. *Chem. Mater.* **2008**, *20*, 26.
(43) Yin, Y.; Erdonmez, C. K.; Cabot, A.; Hughes, S.; Alivisatos, A. P. Colloidal Synthesis of Hollow Cobalt Sulfide Nanocrystals. *Adv. Funct. Mater.* **2006**, *16*, 1389.
(44) Jung, H.-G.; Hassoun, J.; Park, J.-B.; Sun, Y.-K.; Scrosati, B. An improved high-performance lithium−air battery. *Nat. Chem.* **2012**, *4*, 579.
(45) Zahoor, A.; Christy, M.; Jang, H.; Nahm, K. S.; Lee, Y. S. Increasing the reversibility of $Li-O_2$ batteries with caterpillar structured $\alpha-MnO_2$/N−GNF bifunctional electrocatalysts. *Electrochim. Acta* **2015**, *157*, 299.
(46) Padbury, R.; Zhang, X. Lithium−oxygen batteries—Limiting factors that affect performance. *J. Power Sources* **2011**, *196*, 4436.
(47) Xu, D.; Wang, Z.-l.; Xu, J.-j.; Zhang, L.-l.; Zhang, X.-b. Novel DMSO-based electrolyte for high performance rechargeable $Li-O_2$ batteries. *Chem. Commun.* **2012**, *48*, 6948.
(48) Kraytsberg, A.; Ein-Eli, Y. Review on Li−air batteries-Opportunities, limitations and perspective. *J. Power Sources* **2011**, *196*, 886.
(49) Zeng, Q.; Wang, H.; Fu, W.; Gong, Y.; Zhou, W.; Ajayan, P. M.; Lou, J.; Liu, Z. Band Engineering for Novel Two-Dimensional Atomic Layers. *Small* **2015**, *11*, 1868.
(50) Ding, N.; Chien, S. W.; Hor, T. S. A.; Lum, R.; Zong, Y.; Liu, Z. Influence of carbon pore size on the discharge capacity of $Li-O_2$ batteries. *J. Mater. Chem. A* **2014**, *2*, 12433.
(51) Liang, Y.; Li, Y.; Wang, H.; Zhou, J.; Wang, J.; Regier, T.; Dai, H. Co_3O_4 nanocrystals on graphene as a synergistic catalyst for oxygen reduction reaction. *Nat. Mater.* **2011**, *10*, 780.

DOI: 10.1021/acs.chemmater.5b02364
Chem. Mater. 2015, 27, 5726−5735